Universal Journal of Fluid Mechanics **3 (2015), 19-32**
www.papersciences.com

Vortex Shedding for Flow Past Circular Cylinder: Effects of Initial Conditions

Mouna Laroussi, Mohamed Djebbi
Laboratory of Hydraulics and Environment Modeling (LMHE)
National School of Engineers of Tunis (ENIT), University of El-Manar (UM),
B.P. 37, Le Belvédère, 1002 Tunis, Tunisia
mm.lmhe.enit@gmail.com

Abstract
Physically, when the Reynolds number exceeds some critical value, vortex shedding past a circular cylinder appears naturally and immediately. Numerically, vortex shedding requires a long run-time, especially at low Reynolds numbers. In order to reduce this run-time, authors act on either boundaries or initial conditions. The present study tests several forms of initial conditions perturbation. For two blockage ratio 0.1 and 0.05, two-dimensional laminar flow simulations are performed at Re = 100 using the Ansys CFX 12 © finite-element-based finite volume code. Each of the tested forms triggers the vortex shedding after a reasonable time. The time of the onset of periodic shedding is observed using time varying lift coefficient. The run time gained depends on the perturbation form and amplitude. For periodic perturbations, the saved time is even more important than the lateral gradient on the cylinder of the stream-wise velocity is large.

Key Word and Phrases
Vortex Shedding, Low Reynolds Numbers, Initial Conditions Perturbations, Ansys CFX, Run Time Reduction, Non-periodic Perturbations, Periodic Perturbations.

1. Introduction

In the last four decades, there has been a significant growth in the numerical study of bluff body flows, which is characterized by flow separation that produces convective and absolute instabilities. The most well-known instability is that leading to the periodic formation and shedding of spanwise vortices which produce an impressive vortex shedding pattern, namely the von Kármán vortex sheet. The bluff body flow is mainly controlled by the Reynolds number, $Re= U_{\infty}.D/\nu$, where ν is the kinematic viscosity of the fluid which is moving with free-stream velocity U_{∞} and D is the bluff body dimension.

The flow past a circular cylinder is a prototype often employed to study bluff body flows. Physically, when the Reynolds number exceeds some critical value, vortex shedding past the cylinder appears naturally and immediately [1], [2]. Numerically, if the domain geometry and the approaching flow conditions are symmetric, vortex triggering requires a long run-time, especially for low Reynolds numbers. The onset of instability is due to the amplification of the truncation and round-off errors, as well as errors due to the numerical scheme and the sweep direction in the solution procedure [3]-[9]. Nevertheless, due to the importance of the vortex shedding phenomenon, numerical simulations are in high demand and are widely used. Computational approaches solve the Navier–Stokes equations, produce the vortex shedding and are able to mimic the physical instabilities [7].

To reduce the simulation time required for vortex shedding behind a circular cylinder at low Reynolds number, and since the origin mechanism by which the vortex is triggered is not yet clear, several perturbation techniques are used. Among the more often used methods, one is to use the method of the impulsive start from potential solution [2], [10]-[13]. Although there is no experimental evidence of a truly impulsive start [14], several authors use this technique to investigate the problem of vortex shedding, namely for low Reynolds number ([12] for Re=40 and 100, [13] for Re=60, 100 and 250). The flow may also be impulsively started by oscillating ([15] for Re=44, 46.5, 47 and 50) or rotating and/or by translating the cylinder ([16] for Re=200).

Besides the impulsive start technique, several authors disturb either the inlet boundary condition or the condition on the cylinder surface. Some of them chose to use the asymmetric perturbation of the inlet condition [3], [8], [17]. While others chose to perturb initially the inlet condition by adding small-amplitude random perturbation [8], [18]. The perturbation can be introduced also on the cylinder condition by the presence of discrete roughness element [11], by rotation [5], [19], [20] or by small surface asymmetry [21]-[23]. Although these artificial excitation methods trigger the vortex shedding generation process in a short time to periodic state, they are source of energy to the system and may influence the modeling results. Therefore, to better approach the physical reality, an important condition is that the disturbance cannot be the source of energy sustaining the flow regime [3].

Due to the existence of the high shear layer near the cylinder surface, the breaking mechanism is caused by Kelvin-Helmholtz instability. This instability leads to a rolling up and to a separation from the surface of the cylinder that result in the formation of the vortex street [11], [24]-[27]. This breaking mechanism is the basic physics concept of vortex formation and the near wake; that can be an origin of technique for triggering vortex. Knowing that this mechanism can occur even at low Reynolds number, its consequences in terms of reducing the run-time required for triggering the ultimate regular periodic regime are investigated in this paper. The work presented here is, therefore, a natural continuation of our previous work in [28]. It includes numerical study of a laminar vortex shedding past a circular cylinder triggered by acting on initial conditions. Instead of starting calculations from a uniform stream-wise velocity, lateral gradient is introduced so that the stream-wise velocity is the sum of the uniform velocity and a lateral perturbation. Fig. 1 illustrates the combined effects of boundary and initial conditions near the cylinder at the beginning of flow simulation without and with lateral perturbation [28].

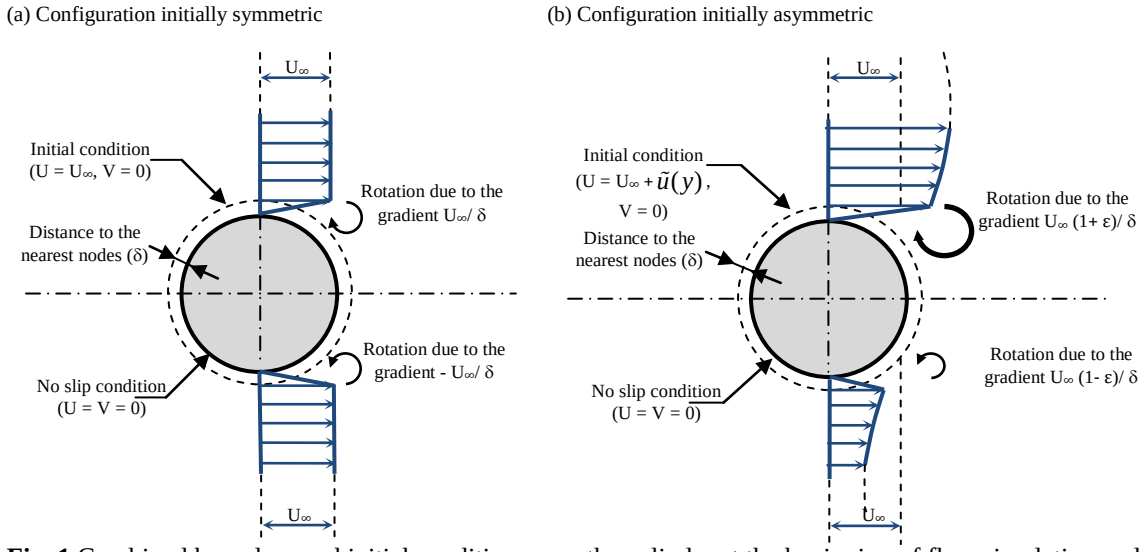

Fig. 1 Combined boundary and initial conditions near the cylinder at the beginning of flow simulation and consequences on the Kelvin-Helmholtz instability [28]

In Fig. 1a, the flow past the cylinder is assumed to start without lateral perturbation. The gradient on both sides of the cylinder surface is symmetric with respect to the horizontal centerline. The corresponding Kelvin-Helmholtz instabilities have same magnitudes and opposite sign and are therefore mutually neutralized. In Fig. 1b, the flow past the cylinder is assumed to start with an asymmetric initial streamwise velocity with lateral gradient. Consequently, and due to lateral gradient, one of the two instabilities is more important than the other and the two instabilities cannot cancel each other. The instability corresponding to the highest gradient imposes a non negligible lateral velocity and form a gradual shear and rotation of the flow in the cylinder vicinity.

Using a lateral 2π-periodic perturbation of the initial streamwise velocity, we previously proved the existence of an optimal value of perturbation amplitude corresponding to a maximum reduction of the simulation time needed to the onset of regular periodic vortex shedding [28]. We found that

for optimal perturbation amplitude, triggering vortex shedding is faster than impulsive start approach and allows obtaining a gain of simulation time of 65%. We also suspected that triggering vortex formation and wake flow may depend on the type of the initial perturbation in addition to its amplitude. The investigation of the effects of these two parameters in reducing the simulation time needed to the onset of regular periodic vortex shedding around a circular cylinder is the main objective of the present study in which issues related to numerical simulation of bluff bodies hydrodynamics in a two dimensional unsteady flows at low Reynolds number of 100, with different periodic and non-periodic lateral perturbation of initial streamwise velocity are presented.

The remainder of the paper is structured as follows. Section 2 presents and describes the numerical methodology. Section 3 summarizes the global time-averaged flow quantities of reference case. Section 4 summarizes the main results of our previous works [28] and discusses the further relevance of the suggested approach. Finally, conclusions and perspectives are presented in Section 5.

2. Numerical Methodology

2.1 Governing Equations

We consider a two-dimensional, unsteady, viscous and incompressible fluid flow with constant properties around a circular cylinder placed in an infinite domain. In a Cartesian coordinating system, the governing equations for mass and momentum conservation are expressed as follow:

$$\frac{\partial u}{\partial x}+\frac{\partial v}{\partial y}=0 \tag{2.1}$$

$$\frac{\partial u}{\partial t}+u\frac{\partial u}{\partial x}+v\frac{\partial u}{\partial y}=-\frac{1}{\rho}\frac{\partial p}{\partial x}+\nu\left(\frac{\partial^2 u}{\partial x^2}+\frac{\partial^2 u}{\partial y^2}\right) \tag{2.2}$$

$$\frac{\partial v}{\partial t}+u\frac{\partial v}{\partial x}+v\frac{\partial v}{\partial y}=-\frac{1}{\rho}\frac{\partial p}{\partial y}+\nu\left(\frac{\partial^2 v}{\partial x^2}+\frac{\partial^2 v}{\partial y^2}\right) \tag{2.3}$$

where, u and v are the streamwise and spanwise velocity components, in the x and y directions, respectively, p is the pressure and t is the time. The dimensionless time τ defined as $\tau = t\cdot U_\infty/D$ will be later used instead of the physical time t.

Eqns (2.1) to (2.3) are solved using the CFD software Ansys CFX.12®. This software achieves a space discretization of the unsteady Navier-Stokes equations with an element based Finite Volume approach in three-dimensional geometry.

The linearized equations are solved using an Algebraic MultiGrid solver [29]-[31]. Tri-linear finite element based functions were used as interpolation scheme for velocity. Linear-Linear finite element based functions were used, as interpolation scheme for pressure. The pressure field is updated each iteration. The pressure-velocity coupling is solved using the Rhie-Chow algorithm [29]. For calculation of the advection terms, the High Resolution scheme was used. In this scheme, the software calculate locally the value of the Blend Factor [29]. In the sake of accuracy, the blend factor will be close to 1.0 for flow regions with low variable gradients (second-order accurate but prone to boundedness problems). In areas where the gradients change sharply, the blend factor will be closer to 0.0 to prevent non-physical values (first-order accurate upwind scheme). For the time discretization of the transient term, we used the Second Order Backward Euler scheme, since it is usually preferable for transient accuracy in CFX rather than the First Backward Euler scheme.

2.2 Computational Domain and Boundary Conditions

Since the domain size influences the solution, a careful selection of the boundary locations becomes vital [32]. The dimensions of the computational domain were then selected with great care to avoid influencing the onset of vortices at the cylinder.

The computational domain dimensions together with the corresponding boundary conditions are depicted on Figure 2. The longitudinal and lateral dimensions of this domain are (Xi + Xe) = 15 times and Xl = 10 times the diameter D of the cylinder, respectively. The cylinder is centered at the origin. The inflow boundary is located at Xi = Xl/2 = 5 times the diameter D of the circular cylinder, while the exit boundary, Xe is placed 10 times the cylinder diameter. The two lateral boundaries are at 5 times on both sides of symmetry axis. The blockage ratio B (ratio of the cylinder diameter to domain width) is then of 0.1. This blockage is enough and is similar to the ratio used in [33]-[36] studies. These defined flow domain dimensions are such that the boundaries of the inflow, the far-field and the out-flow boundaries are located sufficiently far away from the cylinder and therefore do not significantly influence on what happens near the cylinder [37]. To ensure the reliability of our results, a domain with lower blockage ratio of 0.05 (Xi = 10 D and Xl = Xe = 20D) was also studied.

Since all simulations are two-dimensional in the Oxy plane, only one computational cell is used in the vertical direction z and symmetry boundary conditions are applied at the top and the bottom of the 3D computational domain. The other boundary conditions are depicted on Fig.2 and are the following. At the inlet boundary (x = -5D), the magnitude of the inlet uniform velocity U_∞ is specified and the direction is taken normal to the boundary (v = 0). At the outlet boundary (x = 10D), a zero average static pressure (over the whole outlet) is imposed. At the cylinder boundary, the fluid velocity is set to zero (no-slip conditions). The infinite nature of the domain is materialized by considering a wall moving with the same inlet velocity (u = U_∞, v = 0) at the two lateral boundaries (y = ±5D).

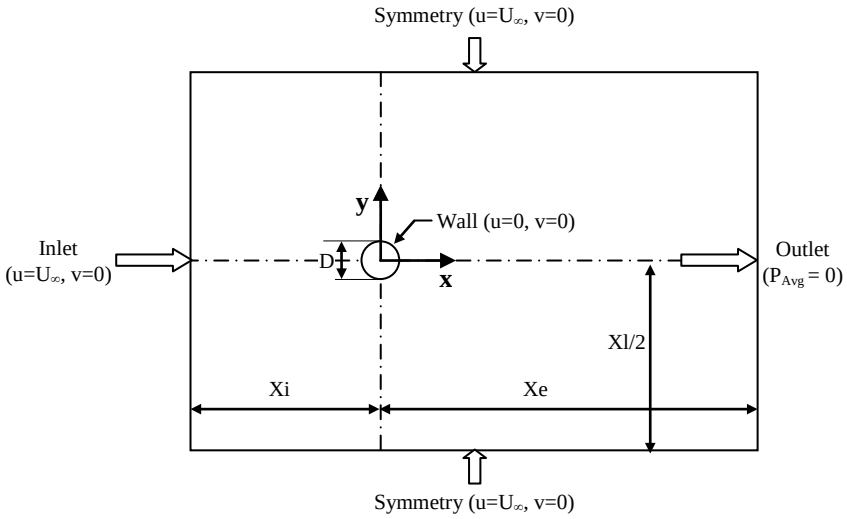

Fig. 2 Computational domain and imposed boundary conditions.

2.3 Initial Conditions

To trigger the onset of flow asymmetry and then minimize transient time, several initial conditions were explored in the present study. These conditions correspond to starting from:

- an impulsive flow with uniform stream-wise velocity (u= U_∞, v=0),
- an impulsive start from the steady state inviscid solution, and

a laterally perturbed stream-wise velocity, with several forms of perturbation functions.

The lateral perturbed stream-wise velocity is expressed as the sum of the uniform velocity, U∞ and a lateral periodic perturbation, $\tilde{u}(y)$ as follows:

$$u(x,y,t=0)=U_{\infty}+\tilde{u}(y) \tag{2.4}$$

In our previous works [28], the lateral perturbation, $\tilde{u}(y)$, is the following 2π-periodic function:

$$\tilde{u}(y)=\alpha U_{\infty}\sin(2\pi\frac{y}{l}) \tag{2.5}$$

where, l is the width of the domain computation and α is the perturbation amplitude coefficient, whose optimal value is expressed as: [28]

$$\alpha_{opt}=\frac{S_t}{2\pi}B^{-1} \tag{2.6}$$

α_{opt} was obtained by equaling the natural vortex shedding frequency with the frequency ∂u/∂y derived from the lateral gradient of the initial stream-wise velocity.

By the present study, the lateral perturbation $\tilde{u}(y)$ will be associated to others perturbation forms. All of the tested forms induce a lateral gradient at the cylinder and generates Kelvin-Helmholtz instability that causes the breaking mechanism. The tested lateral perturbations may be classified in two categories:

(i) Periodic perturbations (Fig. 3) which are expressed as following:

$$\tilde{u}(y)=\alpha U_{\infty}\sin(4\pi\frac{y}{l}) \tag{2.7}$$

$$\tilde{u}(y)=\alpha U_{\infty}\sin(\pi\frac{y}{l}) \tag{2.8}$$

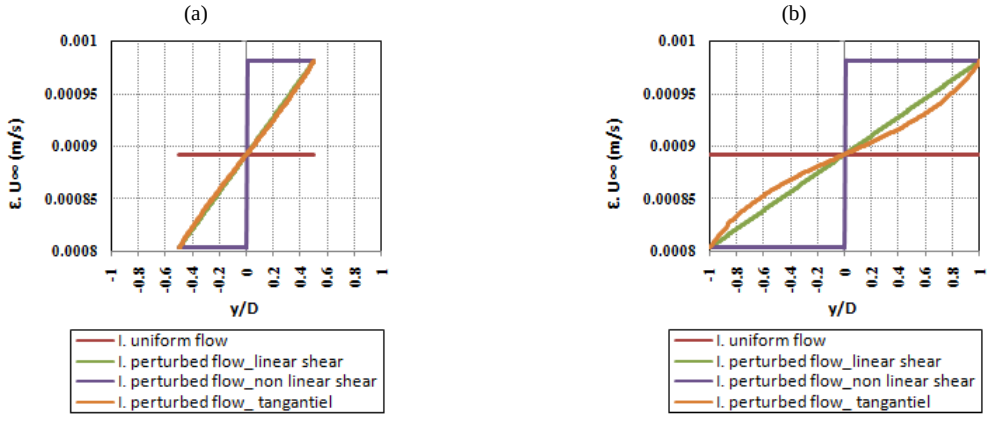

Fig. 3 Sketch profiles of lateral periodic perturbations for different blockage ratio: (a) B=10% and (b) B=5%.

(i) Non-periodic perturbations (Fig. 4) which are expressed as following:

$$\tilde{u}(y)=\alpha U_{\infty}\frac{tan(y)}{\tan(l/2)} \tag{2.9}$$

$$\tilde{u}(y)=\alpha U_{\infty}|y| \tag{2.10}$$

$$\tilde{u}(y)=\alpha U_{\infty}\frac{y}{l/2} \tag{2.11}$$

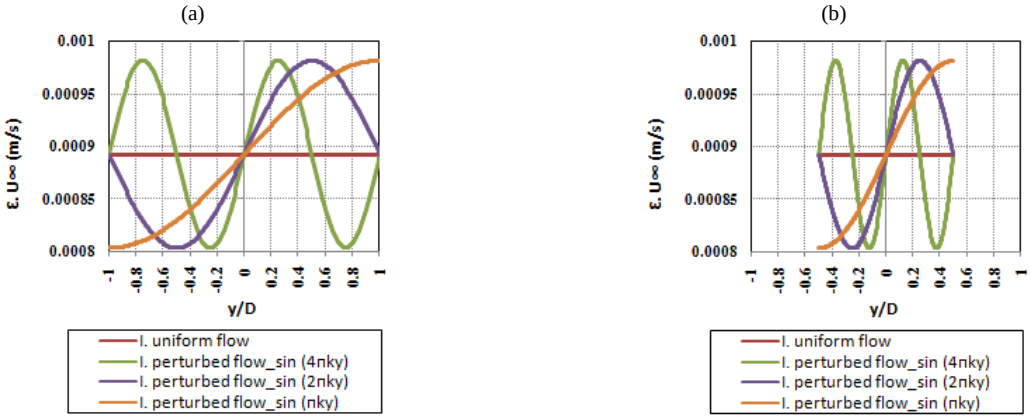

Fig. 4 Sketch profiles of lateral non-periodic perturbations for different blockage ratio: (a) B=10% and (b) B=5%.

For each of the tested lateral perturbations forms, the combined boundary and initial conditions near the cylinder at the beginning of flow simulation is illustrated and sketched in Fig. 5.

(a) I. perturbed flow_sin (π ky) (eq (2.8))

(b) I. perturbed flow_tangential (eq (2.9))

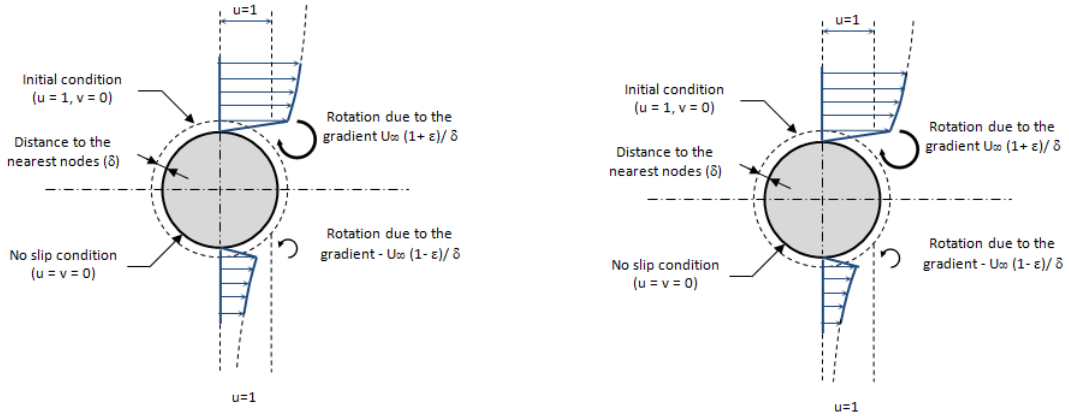

(c) I. perturbed flow_linear shear (eq (2.10))

(d) I. perturbed flow_non-linear shear (eq (2.11))

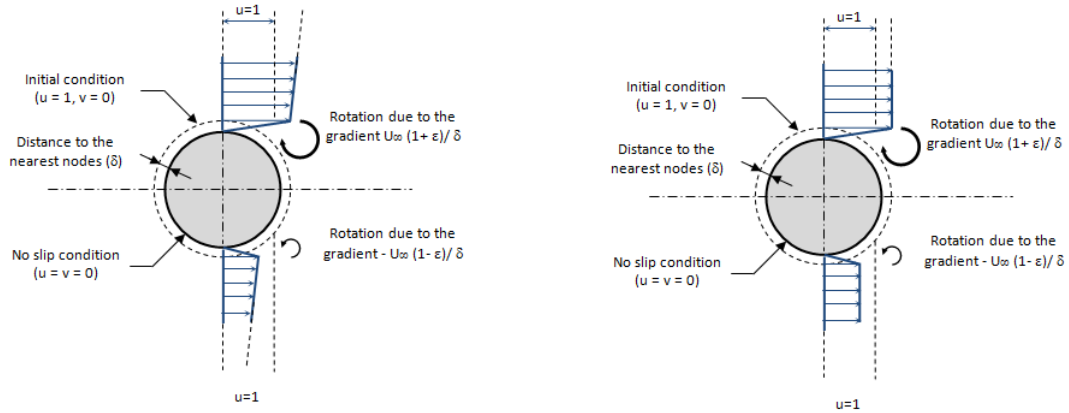

Fig. 5 Combined boundary and initial conditions near the cylinder at the beginning of flow simulation and consequences on the Kelvin-Helmholtz instability in the flow case with configuration initially asymmetric.

2.4. Grid and Time Dependence

The computational domain of the flow field is first divided into structured volumes. The mesh is created using the O-grid and generated using Ansys ICEM. Next it is converted to the unstructured form and then imported to CFX. For the numerical generation of vortex shedding, a very fine mesh in the region close to the cylinder is needed. To achieve this, we covered this region with a block grid system with large dimension and refined this block using O-type Grids: 100 nodes are generated in the circumferential direction and 78 nodes in the normal direction. In order to resolve the flow gradients, the mesh surrounding the cylinder is stretched in the radial direction using the exponential law with distance of the first mesh to the cylinder wall equal to 0.003D.

A grid-independence has been made to ensure the accuracy of the numerical simulations. This preliminary analysis allowed keeping a mesh containing 18384 total hexahedra and 37260 total nodal points. Also, the results obtained with the retained mesh and those with a mesh almost two times finer are very similar and the maximum relative deviation is less than 1%.

Once the optimal mesh was fixed, a time step convergence study was conducted to find the largest time step compatible with the numerical scheme stability. The conditions necessary to prevent the numerical oscillations are determined from the CFL condition. The time step is chosen in a way that the time discretization error and solution error are minimized. The greatest value of the time step ($\Delta\tau$) was determined to be 0.0045 which was adopted in this study. All simulations in this study were performed using the Solver Ansys-CFX.12 over 60,000 – 80,000 time steps which correspond to more than a 30 vortex shedding cycle. The Residual Target of RMS type is set 10^{-5}.

3. Numerical Verification

The main simulated results obtained for a Reynolds number of 100 are summarized in Table 1 together with the numerical results in [37]-[40] and experimental results in [41]. It is clear that the values we obtained agree reasonably well with experimental results. The slight overestimation of the lift and drag coefficients that we obtained is due to the Rhie-Chow algorithm implemented by default in the Ansys CFX Solver. It should also be noted that the size of the computational domain and its spatial discretization may affect the value of the lift and the drag coefficients.

Table 1 Comparison of computed flow properties to others numerical and experimental results at Re=100.

Authors	C_D	C_L	St
Present results	**1.50 ± 0.02**	**± 0.368**	**0.173**
Muddada & Patnaik (2010)[37]	**1.40**	**-**	**0.170**
Mahir & Altaç (2008)[40]	**1.368 ± 0.029**	**± 0.343**	**0.172**
Meneghini (1993)[39]	**1.52**	**-**	**0.162**
Gresho (1980)[38]	**1.816 ± 0.010**	**-**	**0.180**
Norberg (2003)[41](Exp.)	**-**	**± 0.18 to ± 0.54**	**0.168**

4. Results and Discussions

We consider the two-dimensional unsteady flow past a circular cylinder at low Reynolds numbers of Re = 100. Results are presented for the flow patterns in the near wake and fluid induced forces exerted on the cylinder in response to flows with superimposed periodic and non-periodic perturbations to initial stream-wise velocity. The obtained results will be compared to those obtained using a uniform velocity at the start of simulation.

4.1. Flow Patterns

In this section, results of simulations, the evolution of instantaneous streamlines and lift coefficient, are shown for initial uniform flow and for initial 2π-periodic perturbed flow for a typical run at Re=100. The flow streamlines obtained with an initial uniform flow ($\alpha = 0$) and with a perturbed initial flow (Eq (2.5) and Eq (2.6)) are depicted on Fig.6 and 7, respectively.

Fig.6 shows that the numerical generation of the vortex pattern behind the cylinder passes mainly through three phases: (i) flow structure with symmetrical twin vortex that grows with time, (ii) transition to an asymmetrical twin vortex pattern followed by the vortex shedding process, and (iii) fully developed stationary flow with periodic vortex shedding.

Besides, Fig.7 shows that the introduction of an initial lateral streamwise gradient leads to the complete disappearance of phase (i) and to deep changes in phase (ii). However, in a more or less long time, all the simulated cases converge to the same stationary periodic solution (Phase (iii)).

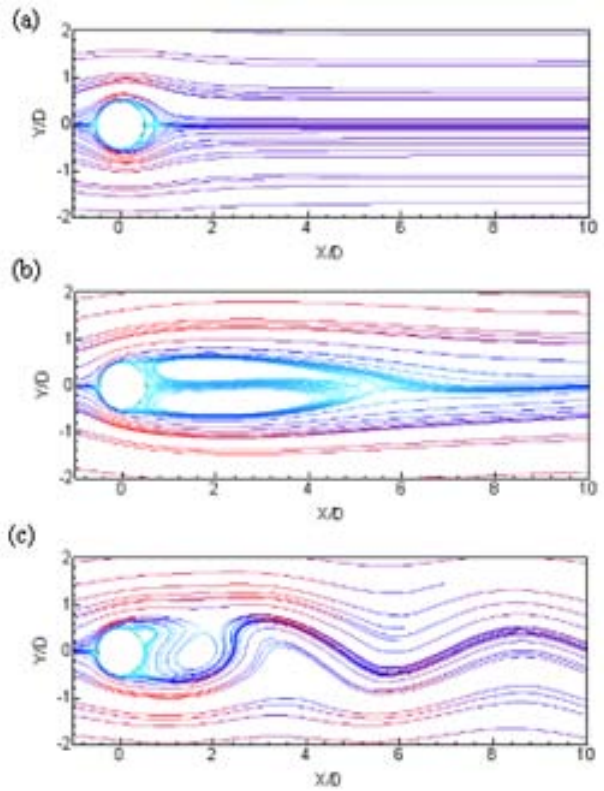

Fig. 6 Streamlines distributions in the cylinder wake at Re=100 at different dimensionless time: (a) 0.71, (b) 47.25 and (c) 138.17.

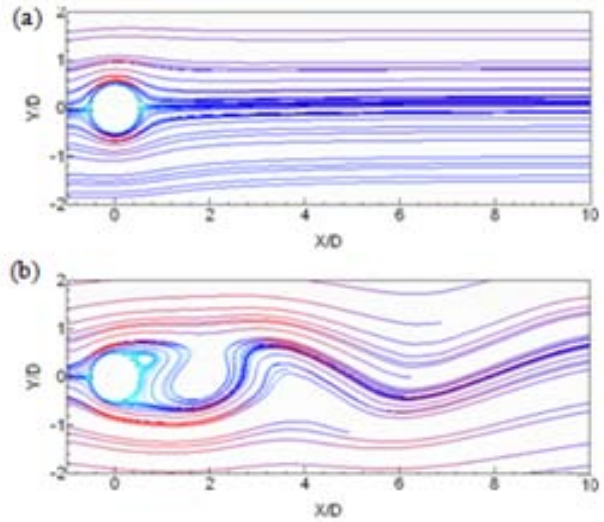

Fig. 7 Streamlines distributions in the cylinder wake at Re=100 at different dimensionless time: (a) 0.54 and (b) 47.25.

The time evolutions of the lift coefficient obtained with an initial uniform flow ($\alpha = 0$) and with a perturbed initial flow (eq (5) and eq (6)) are depicted on Fig.8. Fig.8a shows that the phases (i) and (ii) durations are about 47 and 68 and the total non-dimensional duration of these two phases is therefore 115. Comparing these evolutions to the flow dynamics in Fig.8b, the phases (ii) duration is reduced to about 40.

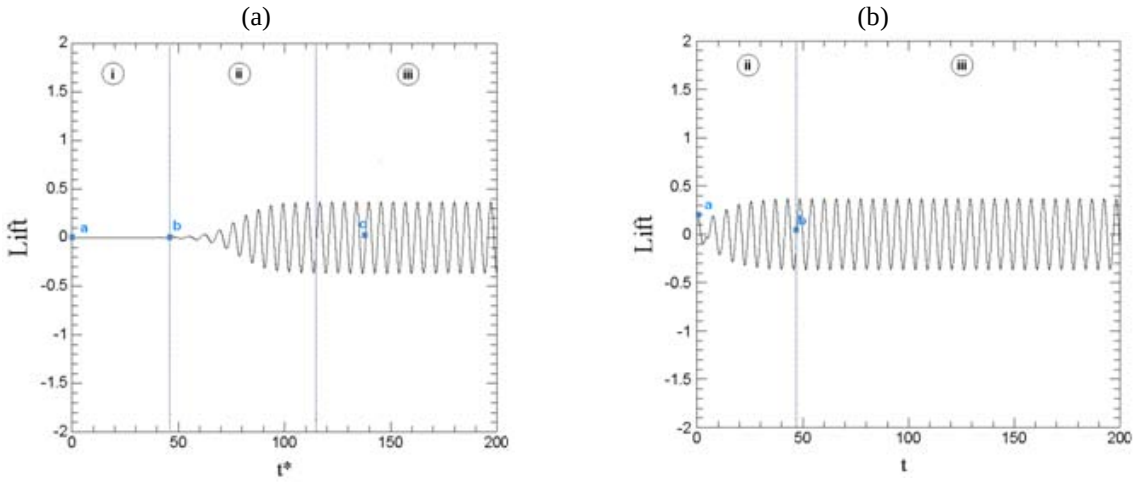

Fig. 8 Instantaneous dimensionless lift force at Re=100 using:
(a) initial uniform flow and (b) initial perturbed flow (eq (2.5) and eq (2.6)).

4.2. Comparison with the Commonly used Impulsive Start Technique

Fig.9 compares the efficiency of the technique, where the initial condition is expressed with α_{opt} (eq (2.5) and eq (2.6)) to the impulsive start from rest technique, where the initial condition is given by the potential flow. Compared to the results of the reference case started with uniform initial velocity, the obtained results show that the impulsive start from rest method is effective and allows a reduction of the time needed for the onset of vortex shedding. However, this reduction is small compared to the time reduction induced by our proposed technique.

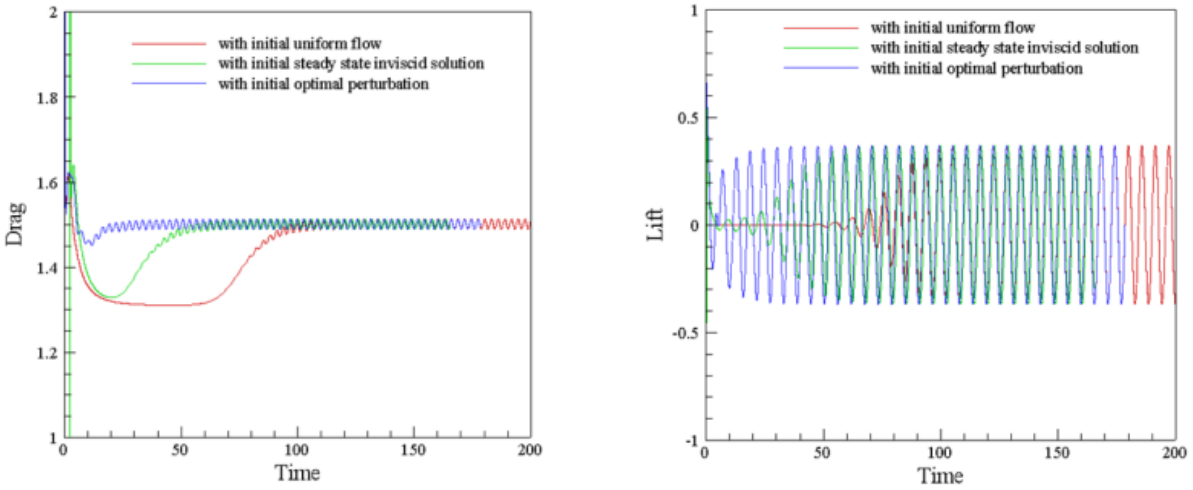

Fig. 9 Instantaneous drag and lift coefficients of flow at Re=100 with an initial uniform flow, with initial steady state inviscid solution and with initial optimal perturbation.

4.3. Reduction of the Flow Simulation Time

The dimensionless time needed to reach the onset of the stationary periodic vortex shedding is 115.1 when starting with uniform initial velocity, 75.4 (i.e. 34.5% of time reduction) when using the impulsive start technique and 40.3 (i.e. 65% of time reduction) when introducing an optimal perturbation of the initial conditions according to (Eq. (2.6)) (see Fig.10).

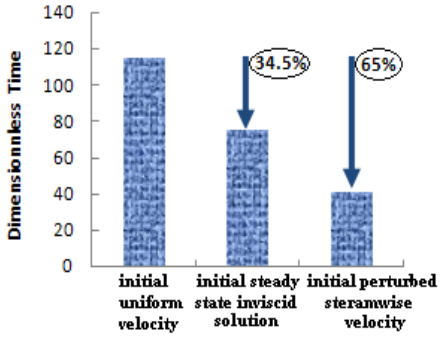

Fig. 10 Time reduction rate for flow past a circular cylinder at Re=100 obtained using initial steady state inviscid solution and with initial optimal perturbation.

4.4. Effect of Periodic Initial Flow Perturbations

Fig.11 shows the evolution of the Maximum Time Reduction rate obtained using different periodic perturbations in initial flow velocity (eq (2.5), eq (2.7) and eq (2.8)) for a domain with a two blockage ratio of 10% and 5%. It is well observed in this figure that the lateral perturbation of the initial stream-wise velocity with 4π-periodic function or 2π-periodic or even π-periodic is more effective than both the initial uniform flow and the initial potential solution, where the time gain exceeds at least 65% compared to initial uniform flow and 32% compared to initial potential solution. However, the period of periodic functions do not significantly affect this gain of time. Passing from Π- period to 4Π-period for a perturbation, the gain of time vary gradually between 64% and 70% for B=10% and between 67% and 73% for B=5%.

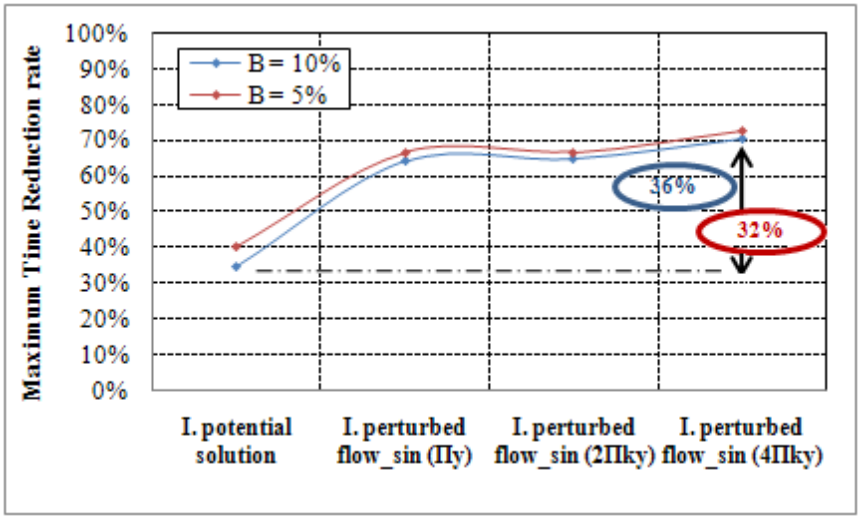

Fig. 11 Maximum Rime reduction rate for flow past a circular cylinder at Re=100 obtained using different periodic perturbation in initial velocity for B=5% and 10%.

We thought to link the different resulted rates of time gain to the gradient on cylinder relatively to each forms of periodic initial conditions. As shown in Fig. 12, a very good quality of the

correlations is obtained in a flow domain with both blockage ratio of 10% and 5%. The gain of time increases progressively with the increases of the gradient at cylinder. This allows resulting that the proposed expression of the periodic initial perturbation (eq (2.5), eq(2.7) and eq(2.8)) with the optimal value α_{opt} (eq (2.6)) implicitly incorporates the gradient at cylinder.

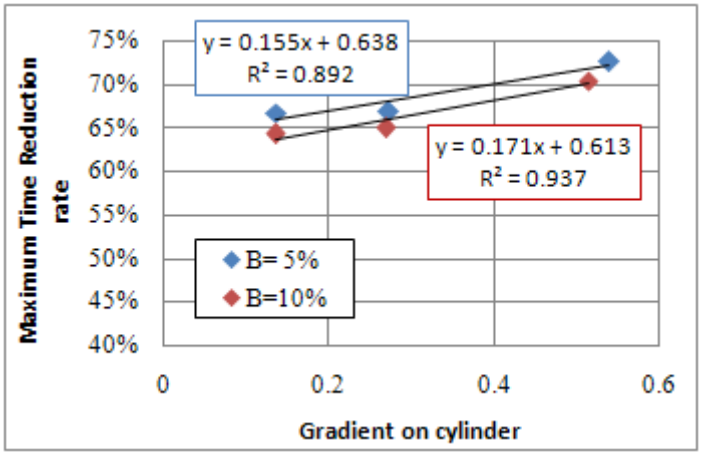

Fig. 12 Evolution of Maximum Time Reduction rate obtained using periodic initial flow perturbations VS Gradient on the cylinder.

4.5. Effect of Non-periodic Initial Flow Perturbations

Fig.13 shows the evolution of the Maximum Time Reduction maximum rate obtained using different non-periodic perturbations in initial flow velocity (eq (2.9), eq (2.10) and eq (2.11)) for a domain with a two blockage ratio of 10% and 5%. It is well observed in this figure that the lateral perturbation of the initial stream-wise velocity is more helpful to trigger vortex shedding; especially when the function of lateral perturbation is non-linear shear or tangential, where the time gain exceeds at least 60% compared to initial uniform flow and 10%, compared to initial potential solution.

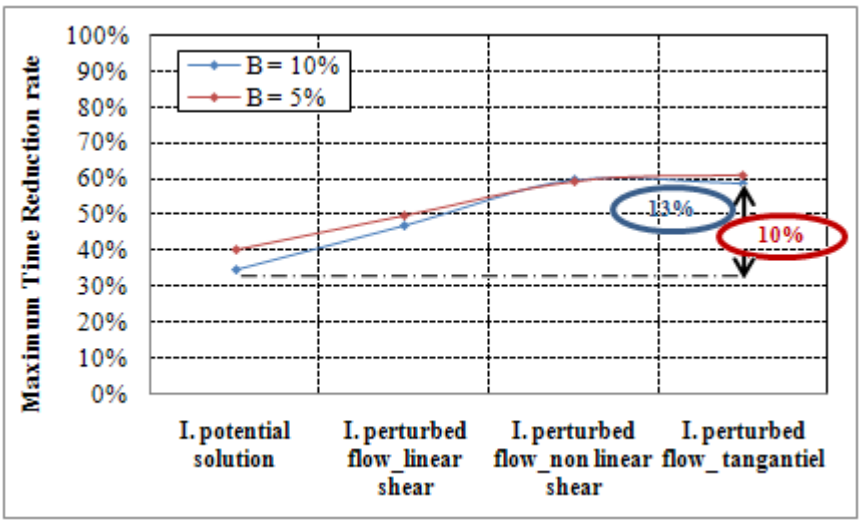

Fig. 13 Maximum Time Reduction rate for flow past a circular cylinder at Re=100 obtained using different non-periodic perturbation in initial velocity for B= 5% and 10%.

Fig.14 shows for both domain with blockage ratio of 10% and 5%, the obtained correlations between the obtained Maximum Reduction Time and the gradient on the cylinder. A poor quality of these correlations is well observed indicating that the proposed expression of the non-periodic initial perturbation with the optimal value α_{opt} doesn't incorporate the gradient at cylinder.

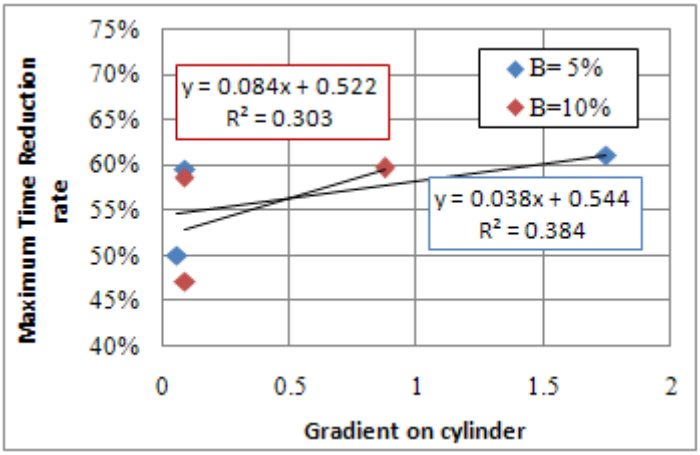

Fig. 14 Evolution of Maximum Time Reduction rate obtained using non-periodic initial flow perturbations VS Gradient on the cylinder.

However, given that the gradient is not regular in the condition where perturbation with non-linear shear function, we propose to adjust the Maximum Time Reduction rate with the gradient on the cylinder, that's obtained using all tested perturbation functions excepted the function (eq(2.11)). As shown in Fig.15, despite all kinds of functions describing the different perturbations with regular gradient at the cylinder, the search for linearity, doesn't sufficient in explaining the variation of CFD simulation reduced time using lateral periodic and non-periodic perturbation, although the strong correlation coefficients that are obtained using the lateral periodic perturbation. Finally, the idea of the gradient at the cylinder based on the rate of reducing the time simulation is to strengthen for the case where the perturbation is periodic as the linear adjustment is better, leading to an improved correlation coefficient (R^2 = 0.892 for B = 10% and R^2 = 0.937 for B = 5%) indicating a good relationship between explained variable and predictor.

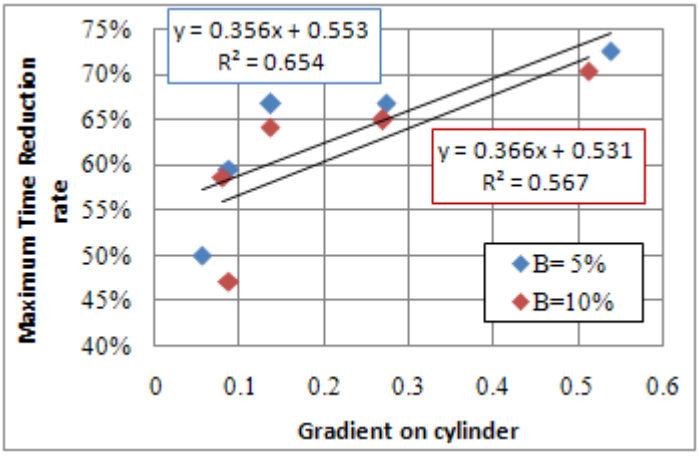

Fig. 15 Maximum Time Reduction rate VS Gradient on cylinder for flow past a circular cylinder at Re=100 and for B= 10% and 5%.

5. Conclusions

Two-dimensional simulations of unsteady flow past a circular cylinder at Re = 100 in an infinite domain were performed for two blockage ratio using as initial conditions (i) uniform stream-wise velocity, (ii) potential solution and (iii) laterally perturbed stream-wise velocity. Each simulation was carried out until the fully developed stationary flow with periodic vortex shedding is reached. Results show that the lateral perturbation of the initial stream-wise velocity triggers very quickly vortex shedding mechanism, especially when the perturbation is periodic. This result confirms that the vortex shedding is caused by Kelvin–Helmholtz instability. The maximum run time reduction is obtained when the natural vortex shedding frequency is equal to the frequency derived from the lateral gradient of the initial stream-wise velocity. Is it a phenomenon of resonance? This is the question we try to answer in a later work.

References

1. *Bouard R. and Coutanceau M.,* 'The early stage of development of the wake behind an impulsively started cylinder for $40 < Re < 10^4$', *J. Fluid Mech.,* ***110*** *(1980), 583 – 607.*
2. *Sengupta T.K. and Sengupta R.,* 'Flow past an impulsively started circular cylinder at high Reynolds number, *Comp. Mech.,* ***14*** *(1994), 298 – 310.*
3. *Afanasyev Y.D. and Korabel V.N.,* 'Wakes and vortex streets behind a localized force: Numerical simulations', *Comm. Nonlin. Scien. Num. Sim.,* ***13*** *(2008), 1101– 1111.*
4. *Bouchon F., Dubois T. and James N.,* 'A second-order cut-cell method for the numerical simulation of 2D flows past obstacles', *Comp. Fluids,* ***65*** *(2012), 80– 91.*
5. *Braza M., Chassaing P. and H.M. H.,* 'Numerical study and physical analysis of the pressure and velocity fields in the near wake of a circular cylinder', J. *Fluid Mech,,* ***166*** *(1986), 79– 130.*
6. *Harichandan A.B. and Roy A.,* 'Numerical investigation of low Reynolds number flow past two and three circular cylinders using unstructured grid CFR scheme', *Int. J. Heat Fluid Flow,* ***31****(2010), 154–171.*
7. *Niazmand H. and Renksizbulut M.,* 'Surface effects on transient three-dimensional flows around rotating spheres at moderate Reynolds numbers', *Comp. Fluids,* ***32*** *(2003),1405– 1433.*
8. *Tamaddon-Jahromi H.R., Townsend P. and Webster M.F.,* 'Unsteady viscous flow past a flat plate orthogonal to the flow', *Comp. Fluids,* ***23*** *(1994), 433– 446.*
9. *Zhang X., Ni S. and He G.,* 'A pressure-correction method and its applications on an unstructured Chimera grid', *Comp. Fluids,* ***37*** *(2008), 993– 1010.*
10. *Collins W.M. and Dennis S.C.R.,* 'Flow past an impulsively started circular cylinder', J. *Fluid Mech.,* ***60*** *(1973), 105– 127.*
11. *Nair M.T. and Sengupta T.K.,* 'Onset of asymmetry: Flow past circular and elliptic cylinders', *Int. J. Num. Meth. Fluids,* ***23*** *(1996), 1327– 1345.*
12. *Payne R.B.,* 'Calculations of unsteady viscous flow past a circular cylinder', *J. Fluid Mech.,* ***4*** *(1958), 81– 86.*
13. *Sengupta T.K., Singh N. and Suman V.K.,* 'Dynamical system approach to instability of flow past a circular cylinder', *J. Fluid Mech.,* ***656*** *(2010), 82– 115.*
14. *Koumoutsakost P. and Leonard A.,* 'High-resolution simulations of the flow around an impulsively started cylinder using vortex methods', *J. Fluid Mech.,* ***296****(1995),1– 38.*
15. *Kalita J.C. and Sen S.,* 'Triggering asymmetry for flow past circular cylinder at low Reynolds numbers', *Comp. Fluids,* ***59*** *(2012), 44– 60.*
16. *Badr H.M. and Dennis S.C.R.,* 'Time dependent viscous flow past an impulsively started rotating and translating circular cylinder', *J. Fluid Mech.,* ***158*** *(1985), 447– 488.*
17. *Lecointe Y. and Piquet J.,* 'On the use of several compact methods for the study of unsteady incompressible viscous flow around a circular cylinder', *Comp. Fluids,* ***12****(1984), 255 – 280.*
18. *Yoshida Y. and Nomura T.,* 'A transient solution method for the finite element incompressible navier-stokes equations', *Int. J. Num. Meth. Fluids,* ***5*** *(1985), 873– 890.*
19. *Al-Mdallal Q.M., Lawrence K.P. and Kocabiyik S.,* 'Forced streamwise oscillations of a circular cylinder: Locked-on modes and resulting fluid forces', *J. Fluids Struct.,* ***23*** *(2007), 681– 701.*
20. *Zhao M., Cheng L., Teng B. and Liang D.,* 'Numerical simulation of viscous flow past two circular cylinders of different diameters', *App. Ocean Res.,* ***27*** *(2005), 39– 55.*
21. *Hartwich P.M., Halt R.M. and Hemschs M.J.,* 'Navier-Stokes computations of vortex asymmetries controlled by small surface imperfections', *in 28th Aerospace Sciences Meeting, (1991), 258– 264.*

22. *Levy Y., Hesselinky L. and Deganiz D.,* 'A systematic study of the correlation between Geometrical Disturbances and Flow Asymmetries', *in 33rd Aerospace Sciences Meeting and Exhibit, (1995).*
23. *Murman S.M.,* 'Geometric Perturbations and Asymmetric Vortex Shedding about Slender Pointed bodies', *Atmospheric Flight Mechanics Conference, (2000).*
24. *Muti Lin J.C. and Pauley L.L.,* 'Low-Reynolds-Number Separation on an Airfoil', *AIAA Journal, **34** (1996), 1570– 1577.*
25. *Nishioka M. and Sato H.,* 'Mechanism of determination of the shedding frequency of vortices behind a cylinder at low Reynolds numbers', *J. Fluid Mech., **89** (1978), 49– 60.*
26. *Posdziecha O. and Grundmann R.,* 'A systematic approach to the numerical calculation of fundamental quantities of the two-dimensional flow over a circular cylinder', *J. Fluids Struct., **23** (2007), 479– 499.*
27. *Sumer B.M. and Fredsoe J., 'Hydrodynamics around cylindrical structures'*, World Scientific Publishing, *2006.*
28. *Laroussi, M., Djebbi M., and Moussa M.,* 'Triggering vortex shedding for flow past circular cylinder by acting on initial conditions: A numerical study', *Comp. Fluids, **101** (2014), 194– 207.*
29. *Ansys Inc., 'Ansys CFX-Solver Theory Guide'*, USA, *2009.*
30. *Bayraktar E., Mierka O., and Turek S.,* 'Benchmark computations of 3D laminar flow around a cylinder with CFX, OpenFOAM and FeatFlow', *Int. J. Comp. Scien. Engng, (2012).*
31. *Jeong W. and Seong J.,* 'Comparison of effects on technical variances of computational fluid dynamics (CFD) software based on finite element and finite volume methods', *Int. J. Mech. Scien., **78** (2014), 19– 26.*
32. *Ünal U.u.O., Atlar M., and Gören Ö.,* 'Effect of turbulence modeling on the computation of the near-wake flow of a circular cylinder', *Ocean Engng, **37** (2010), 387– 399.*
33. *Vinod A.V. and Ros D.,* 'CFD Simulation of Wall Effects in Flow Past a Circular Cylinder in a Plane Channel', *IE(I) Journal-CH, **89** (2008), 3– 9.*
34. *Węcel D., Chmielniak T., and Kotowicz J.,* 'Experimental and numerical investigations of the averaging Pitot tube and analysis of installation effects on the flow coefficient', *Flow Meas. Instr., **19**(2008), 301– 306.*
35. *Yousefifard M., Ghadimi P. and Zamanian R.,* 'Unstructured Grid Solutions for Incompressible Laminar Flow over a Circular Cylinder Using a Particular Finite Volume-Finite Element Method', *J. Engng, (2013), 1– 9.*
36. *Jackson C.P.,* 'A finite-element study of the onset of vortex shedding in flow past variously shaped bodies', *J. Fluid Mech., **182**(1987), 23– 45.*
37. *Muddada S. and Patnaik B.S.V.,* 'An active flow control strategy for the suppression of vortex structures behind a circular cylinder', *Europ. J. Mech. - B/Fluids, **29** (2010), 93– 104.*
38. *Gresho P.M., Lee R.L. and Sani R.L.,* 'On the time-dependent solution of the incompressible Navier-Stokes equations in two and three dimensions', *Rec. Adv. Num. Meth. Fluids, **1**(1980), 27– 79.*
39. *Meneghini J.R., 'Numerical simulation of bluff body flow control using a discrete vortex method'*, PhD thesis, University of London, U.K, *1993.*
40. *Mahír N. and Altaç Z.,* 'Numerical investigation of convective heat transfer in unsteady flow past two cylinders in tandem arrangements', *Int. J. Heat Fluid Flow, **29** (2008), 1309– 1318.*
41. *Norberg C.,* 'Fluctuating lift on a circular cylinder: review and new measurements', *J. Fluids Struct., **17** (2003), 57– 96.*